IUScholarWorks at Indiana University South Bend

Selective Population and Neutron Decay of the First Excited State of Semi-Magic 23O

Schiller A, Frank N, Baumann T, Bazin D, Brown BA, Brown J, DeYoung PA, Finck JE, Gade A, Hinnefeld J, Howes R, Lecouey JL, Luther B, Peters WA, Scheit H, Thoennessen M, Tostevin JA

Selective population and neutron decay of the first excited state of semi-magic ^{23}O

A. Schiller,[1, *] N. Frank,[1, 2, 3] T. Baumann,[1] D. Bazin,[1] B.A. Brown,[1, 2] J. Brown,[4]
P.A. DeYoung,[5] J.E. Finck,[6] A. Gade,[1, 2] J. Hinnefeld,[7] R. Howes,[8] J.-L. Lecouey,[1, †]
B. Luther,[3] W.A. Peters,[1, 2] H. Scheit,[1] M. Thoennessen,[1, 2] and J.A. Tostevin[1, 2, 9]

[1]*National Superconducting Cyclotron Laboratory, Michigan State University, East Lansing, MI 48824*
[2]*Department of Physics & Astronomy, Michigan State University, East Lansing, MI 48824*
[3]*Department of Physics, Concordia College, Moorhead, MN 56562*
[4]*Department of Physics, Wabash College, Crawfordsville, IN 47933*
[5]*Department of Physics, Hope College, Holland, MI 49423*
[6]*Department of Physics, Central Michigan University, Mt. Pleasant, MI 48859*
[7]*Department of Physics & Astronomy, Indiana University at South Bend, South Bend, IN 46634*
[8]*Department of Physics, Marquette University, Milwaukee, WI 53201*
[9]*School of Electronics and Physical Sciences, University of Surrey, Guildford GU2 7XH, UK*

We have observed an excited state in the neutron-rich semi-magic nucleus ^{23}O for the first time. No such states have been found in previous searches using γ-ray spectroscopy. The observation of a resonance in n-fragment coincidence measurements confirms the speculation in the literature that the lowest excited state is neutron unbound and establishes positive evidence for a 2.8(1) MeV excitation energy of the first excited state in ^{23}O. The non-observation of a predicted second excited state is explained assuming selectivity of inner-shell knockout reactions.

PACS numbers: 21.10.Pc, 23.90.+w, 25.60.Gc, 29.30.Hs

Magic numbers are pillars of our understanding of nuclear structure. For each magic number of nucleons one can observe, e.g., (i) a large number of stable isotopes or isotones, large binding energies, and corresponding structures in separation-energy systematics, (ii) increased excitation energies of first excited states for even-even nuclei, and a corresponding reduction of their ground-state transition matrix elements, and (iii) a decreased level density at low and moderate excitation energies [1]. Nuclei with one nucleon added or removed from a doubly-magic core are well described by a single-particle (SP) model; their properties such as spins and parities, magnetic moments, energies of the lowest excited states, and transition matrix elements are well reproduced by SP estimates. The underlying physics for the emergence of magic numbers is the presence of gaps in the SP spectrum around the Fermi energy, which makes the last nucleon tightly bound whereas any additional nucleons will be loosely bound. If the energy gaps are larger than the strength of residual interactions such as pairing or quadrupole-quadrupole interactions, only weak correlations of such types are induced, hence, no corresponding low-lying collectivity is observed.

Magic numbers for stable nuclei follow harmonic-oscillator shells up to $N, Z = 20$; for heavier nuclei, the spin-orbit splitting between high-l orbitals produces $N, Z = 28$, 50, 82, and 126. The emergence of new magic numbers far from stability is thought to be related to the effect of the tensor force [2], which produces (among others) attractive contributions for $0d_{3/2}$ neutrons in the presence of $0d_{5/2}$ protons. For oxygen isotopes the proton $0d_{5/2}$ orbit is not occupied. This contributes to the reduced binding of the $\nu(0d_{3/2})$ orbital

[3] and produces a gap at $N = 16$, while for stable nuclei the gap at $N = 16$ disappears since the $0d_{5/2}$ proton shell is almost filled. The effect of the occupation number on SP spectra is taken into account by considering effective SP (ESP) energies, where SP energies are modified by the average monopole contribution of residual interactions. The neutron ESP spectra for neutron-rich oxygen isotopes derived with the universal sd-shell (USD) interaction (which takes into account the effects of residual forces by virtue of a fit to experimental data) reveal large gaps for ^{22}O and ^{24}O at the Fermi energy. Both nuclei are predicted to be doubly magic with $N = 14$ and 16, respectively [4]; hence, the properties of ^{23}O are expected to be well reproduced by a SP description. In ^{22}O, a high-lying first excited state has been observed in γ-ray spectroscopy [5] confirming the magic character of $N = 14$ for $Z = 8$. Systematics of neutron separation energies suggest a magic character of $N = 16$ at the neutron dripline [6], but no high-lying first excited state has been found for ^{24}O [5]. Focusing on the SP nucleus ^{23}O, we have populated the n-^{22}O continuum by $2p + 1n$ removal from a ^{26}Ne beam and deduced the decay-energy spectrum of excited ^{23}O in order to search for resonances corresponding to unbound states. Two-proton knockout reactions have proven to be a sensitive tool to study nuclear structure of rare isotopes [7]. These direct reactions rely on the knockout of valence protons leaving the remaining nucleons largely undisturbed. In the present paper, direct knockout of inner-shell protons is utilized for the first time to observe neutron-unbound states in neutron-rich nuclei. It is shown that these proton hole states couple to specific highly excited neutron states.

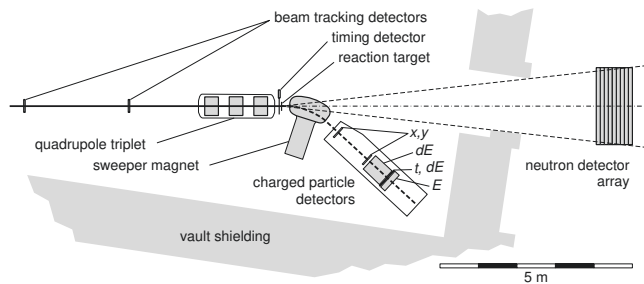The experiment was performed at the National Su-

FIG. 1: Experimental setup for measuring fragment-neutron coincidences at the NSCL. The A1900 and extended focal plane scintillator are upstream and not shown here.

FIG. 2: a) Energy loss in thin scintillator vs. ion chamber provides Z identification. b) TKE in thick scintillator vs. corrected ToF for oxygen fragments provides isotope identification. c) Neutron ToF for decay of $^{23}O^*$, i.e., in coincidence with ^{22}O fragments, and using a thick target in singles mode showing prompt γ radiation (inset). The 1.4 ns FWHM of the γ peak translates into a n-energy resolution of 1.4 MeV. d) Data in b) projected onto the diagonal line.

perconducting Cyclotron Laboratory (NSCL) at Michigan State University. A 105 pnA primary beam of 140 MeV/A ^{40}Ar impinged on a 893 mg/cm^2 Be production target. The resulting cocktail beam was purified with respect to the desired ^{26}Ne at 86 MeV/A using an achromatic 750-mg/cm^2-thick acrylic wedge degrader and either 1% or 3% momentum-acceptance slits at the dispersive focal plane for different parts of the experiment, as well as ± 10 mm slits at the extended focal plane of the A1900 fragment separator [8]. A purity of up to 93.2% was achieved with a ^{26}Ne beam intensity of about 7000 pps. The contaminants (mainly ^{27}Na and ^{29}Mg) were separated event-by-event in the offline analysis by their different time-of-flight (ToF) from the extended focal plane to the scintillator in front of the 721-mg/cm^2-thick Be reaction target (see Fig. 1). Positions and angles of incoming beam particles were measured by two 15×15 cm^2 position-sensitive parallel-plate avalanche counters (PPACs) with 20 pads/inch, i.e., FWHM ≈ 1.3 mm. Due to the focusing of the quadrupole triplet, positions of impinging ^{26}Ne particles on the reaction target could be reconstructed within a radius of $\sigma_r = 1$ mm.

Charged particles behind the reaction target were bent $43°$ by the large-gap 4 Tm Sweeper Magnet [9]. Two 30×30 cm^2 cathode-readout drift chambers (CRDCs) provided position in the dispersive (10 pads/inch, $\sigma_x \approx 1.1$ mm) and non-dispersive (drift time, $\sigma_y \approx 1.3$ mm) direction. The 1.87 m distance between the CRDCs translates this into $\sigma = 1$ mrad angle resolution. Energy loss was determined in a 65-cm-long ion chamber (IC) and a 40×40 cm^2, 4.5-mm-thin plastic scintillator whose pulse-height signal was corrected for position. Energy loss was used to separate reaction products with different Z (see Fig. 2a). The thin scintillator also gave ToF of reaction products from the reaction target. This, together with the total kinetic energy (TKE) measurement in a 15-cm-thick plastic scintillator, provided isotopic separation (see Fig. 2b, d). The pulse-height signal of the thick scintillator was also corrected for position; the raw ToF was corrected for (i) position on the thin scintillator, for (ii)
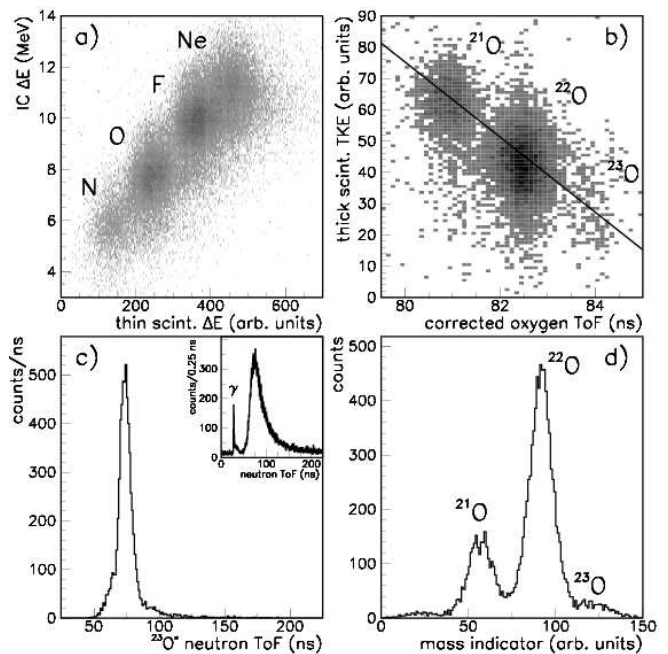
angle and position behind the Sweeper Magnet, as well as for (iii) the point of interaction on the target. The ToF corrections approximately compensate the spread in energy of reaction products and account for differences in length of the fragment tracks and of the light paths in the thin scintillator. Due to the finite acceptance a magnetic-rigidity range of reaction products is selected. For reaction products with equal Z, this translates into TKE $\propto 1/A$ and ToF $\propto A$ (see Fig. 2b).

Neutrons were detected in the Modular Neutron Array (MoNA) [10] at a distance of 8.2 m from the reaction target. MoNA consists of 9×16 stacked 2-m-long plastic scintillator bars which are read out on both ends by photomultiplier tubes (PMT). The bars are mounted horizontally and perpendicular to the beam axis. Position along the vertical and along the beam axis is determined within the thickness of one bar (10 cm, $\sigma \sim 3$ cm). Horizontal position and neutron ToF are determined by the time difference and the mean time, respectively, of the two PMT signals which yield resolutions of $\sigma \approx 5$ cm and $\sigma \approx 0.1$ ns. The ToF spectrum was calibrated by shifting the prompt γ-ray peak from a thick-target MoNA singles run to 27 ns, see inset in Fig. 2c. A neutron ToF spectrum (first hit after ~ 27 ns) in coincidence with ^{22}O fragments is given in Fig. 2c.
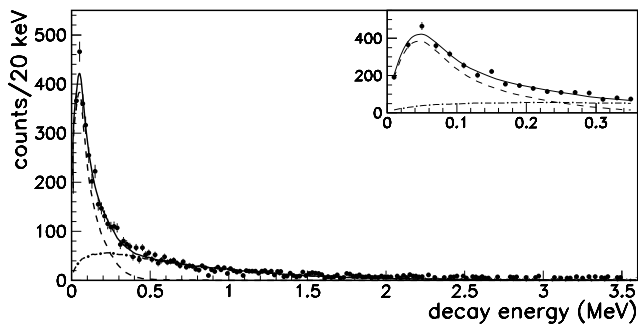
FIG. 3: Decay-energy spectra of ^{23}O*. The inset shows a close-up of the first 360 keV. Smooth curves correspond to simulations (see text). The solid curve corresponds to the sum of the dash-dotted and dashed curves.

FIG. 4: a) Likely configuration of the ^{24}O continuum populated by direct 2p removal from ^{26}Ne. These negative-parity proton excitations will mix with certain negative-parity neutron excitations b), c), which then decay into the ^{23}O ground state or continuum.

The decay energy of resonances is reconstructed by the invariant mass method. For this, the relativistic four-momentum vectors of the neutron and fragment are reconstructed at the point of breakup. For neutrons, position and ToF resolution translate into angle and energy resolution of $\sigma = 8$ mrad and $\sigma = 1.6$ MeV [19], respectively. The angle and energy of fragments in coincidence with neutrons were reconstructed behind the reaction target based on the ion-optical properties of the Sweeper Magnet using a novel method which takes into account the position at the target in the dispersive direction [11]. The reconstructed position in the non-dispersive direction serves thereby as a double check on an event-by-event basis against the same information obtained from forward tracking from the PPACs through the quadrupole triplet. The angle and energy resolution of the fragments behind the target are $\sigma = 2.7$ mrad and $\sigma = 0.4$ MeV/A, respectively. The average energy loss of the fragment through half of the reaction target is added to approximate the relativistic four-momentum vector of the fragment at the average breakup point.

The experiment ran for two days and produced 5700 n-^{22}O coincidences. The reconstructed decay-energy spectrum from n-^{22}O coincidences is shown in Fig. 3. This spectrum is affected by the finite acceptance for fragments and neutrons and a bias toward the fastest neutron for events where more than one neutron hit MoNA. The latter is because in the analysis only the first hit after ~ 27 ns is taken into account. Later hits due to either multiple scattering of one neutron or true multiple-neutron events are ignored in the analysis [11]. The most severe of these effects, namely the acceptance cuts, have been simulated. For the simulation, a Glauber reaction model is used. Angle straggling of the fragments in the target is taken into account, as well as detector resolutions. The n-^{22}O data in Fig. 3 are best described by a Breit-Wigner resonance at 45(2) keV decay energy (dashed curve) on top of a beam-velocity source of Maxwellian-distributed neutrons (a thermal model) with
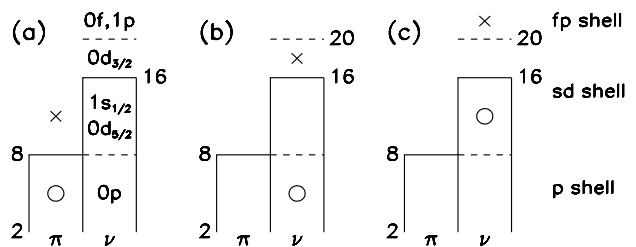
$T \sim 0.7$ MeV (dash-dotted curve). The ratio of the contributions is 1:2. The simulated decay-energy resolution, in qualitative agreement with [12], is found to scale as FWHM $\sim 16\sqrt{E \cdot \text{keV}}$ and $40\sqrt{E \cdot \text{keV}}$, below and above $E = 1.5$ MeV decay energy, respectively. The numerical factors are dominated by n-angle resolution and target thickness, respectively. For the present resonance, the width due to experimental conditions (100 keV) overshadows the Wigner limit by about three orders of magnitude, hence its lifetime is not determined. The thermal model has been included in the fit because it is a good description of uncorrelated events as determined from event mixing, and it serves as an estimate of non-resonant contributions to the decay-energy spectrum (see, e.g., [12, 13] for further discussions of experimental backgrounds).

When combined with the neutron separation energy S_n [14], our result establishes an excitation energy of 2.79(13) MeV for the first excited state of ^{23}O. Two low-lying states with spin-parities of $3/2^+$ and $5/2^+$, based on a $\nu(0d_{3/2})^1$ particle and $\nu(0d_{5/2})^{-1}$ hole configuration, respectively, are predicted by theory [15], with the $5/2^+$ level the lower one and hence being the favored spin-parity assignment for the here observed resonance. Observation of decay to excited states in ^{22}O which are at 3.4 MeV and higher are thought to be unlikely.

The selective population of the states can be understood from the structure of ^{24}O and the specific reaction mechanism. The main component (90%) of the ^{24}O ground-state wavefunction has the closed-shell configuration $[d_{5/2}^6, s_{1/2}^2]$. The ^{26}Ne ground-state wavefunction is dominated by two sd-shell protons coupled to the ground state of ^{24}O [16]. Two-proton removal from ^{26}Ne to the low-lying states in ^{24}O can thus proceed by the removal of two sd-shell protons to the ^{24}O ground state or by one sd-shell and one p-shell proton to the negative-parity configuration shown in Fig. 4a. The negative-parity eigenstates are linear combinations of the three configurations in Fig. 4. The neutron-decay of these eigenstates goes by $d_{3/2}$ neutron decay to high-lying negative parity states (b) and by fp-shell neutron decay to the $1/2^+$ and $5/2^+$

one-neutron-hole states (c) in ^{23}O. Thus, starting with the main component of the ^{26}Ne wavefunction no overlap with the $3/2^+$ $[d^6_{5/2}, d_{3/2}]$ excited state of ^{23}O is possible. The direct reaction theory [17] for the removal of two sd-shell protons from the ^{26}Ne to the ^{24}O ground state gives a cross section of about 0.42 mb where a suppression factor of 0.5 was used [17]. The removal of one proton from the sd-shell and one proton from the fully occupied p-shell (6 protons) corresponds to a total cross section of about 2.1 mb. These states will neutron decay to the low-lying $1/2^+$ and $5/2^+$ states of ^{23}O. In addition, we might expect some direct three-nucleon knockout from removal of two sd-shell protons plus one sd-shell neutron, but again, with the dominant $[d^6_{5/2}, s^2_{1/2}]$ neutron structure of ^{26}Ne this can only go to the $1/2^+$ $[d^6_{5/2}, s^1_{1/2}]$ and $5/2^+$ $[d^5_{5/2}, s^2_{1/2}]$ states of ^{23}O. Population of the $3/2^+$ $[d^6_{5/2}, d_{3/2}]$ state of ^{23}O as well as the 2^+ $[d^6_{5/2}, s_{1/2}, d_{3/2}]$ state of ^{24}O can only come from the small component of the ^{26}Ne ground state with the neutron configuration $[d^6_{5/2}, s_{1/2}, d_{3/2}] \otimes 2^+(\pi)$. With full sd-shell wavefunctions the cross section to the 2^+ state of ^{24}O is 0.03 mb (with the reduction factor of 0.5) compared to 0.42 mb for the ground state. Accordingly, the cross section for the $3/2^+$ state in ^{23}O should be smaller by about an order of magnitude than those for the $1/2^+$ ground and $5/2^+$ excited states.

Considering only the dominant components of the wavefunctions the spectroscopic factor for the neutron decay of the $5/2^+$ $[d^5_{5/2}, s^2_{1/2}]$ state in ^{23}O to the $[d^6_{5/2}]$ ground state in ^{22}O is zero. With the full USDB wavefunctions [18], the spectroscopic factor is 0.059. Thus, with a d-wave neutron single-particle width of 90(10) eV (corresponding to a decay energy of 45(2) keV), the total decay width of 5.0(6) eV is extremely small. Still, the calculated γ-decay lifetime is 4.5 ps corresponding to a partial width of 0.15 meV, hence the decay is dominated by neutrons.

In conclusion, we have observed for the first time an excited state in ^{23}O. This state has been sought for unsuccessfully using γ-ray spectroscopy; due to its unbound nature it is revealed in the present work in an n-fragment coincidence experiment. On the other hand, a predicted second excited state has not been found. This has been explained by the presence of selection effects in the population of states in ^{23}O, which, in return, demonstrates that inner-shell proton knockout is a new promising spectroscopic tool to explore excited states far from stability.

[*] Electronic address: schiller@nscl.msu.edu

[†] Present address: Laboratoire de Physique Corpusculaire, ENSICAEN, IN2P3, 14050 Caen, Cedex, France

[1] Aa. Bohr and B.R. Mottelson, *Nuclear Structure* (Benjamin, New York, 1969), Vol. I, p. 189.

[2] T. Otsuka, T. Suzuki, R. Fujimoto, H. Grawe, and Y. Akaishi, Phys. Rev. Lett. **95**, 232502 (2005); T. Otsuka, T. Matsuo, and D. Abe, *ibid.* **97**, 162501 (2006).

[3] T. Otsuka *et al.*, Phys. Rev. Lett. **87**, 082502 (2001).

[4] B.A. Brown and W.A. Richter, Phys. Rev. C **72**, 057301 (2005).

[5] M. Stanoiu *et al.*, Phys. Rev. C **69**, 034312 (2004).

[6] A. Ozawa, T. Kobayashi, T. Suzuki, K. Yoshida, and I. Tanihata, Phys. Rev. Lett. **84**, 5493 (2000).

[7] D. Bazin *et al.*, Phys. Rev. Lett. **91**, 012501 (2003); D. Warner, Nature **425**, 570 (2003); J. Fridmann *et al.*, *ibid.* **435**, 922 (2005).

[8] D.J. Morrissey, B.M. Sherrill, M. Steiner, A. Stolz, and I. Wiedenhoever, Nucl. Instrum. Methods Phys. Res. **B204**, 90 (2003).

[9] M.D. Bird *et al.*, IEEE Trans. Appl. Supercond. **15**, 1252 (2005).

[10] B. Luther *et al.*, Nucl. Instrum. Methods Phys. Res. **A505**, 33 (2003); T. Baumann *et al.*, *ibid.* **A543**, 517 (2005).

[11] N. Frank, Ph.D. thesis, Michigan State University, 2006.

[12] N. Fukuda *et al.*, Phys. Rev. C **70**, 054606 (2004).

[13] F. Deák, *et al.*, Nucl. Instrum. Methods Phys. Res. **A258**, 67 (1987).

[14] G. Audi, A.H. Wapstra, and C. Thibault, Nucl. Phys. **A729**, 337 (2003).

[15] A. Volya and V. Zelevinsky, Phys. Rev. Lett. **94**, 052501 (2005).

[16] J.R. Terry *et al.*, Phys. Lett. **B 640**, 86 (2006).

[17] J.A. Tostevin and B.A. Brown , Phys. Rev. C **74**, 064604 (2006).

[18] B.A. Brown and W.A. Richter , Phys. Rev. C **74**, 034313 (2006).

[19] The nominal energy resolution of $\sigma = 0.7$ MeV is degraded by a systematic ToF walk with deposited energy. This walk does neither affect the position resolution along a bar, nor can it be corrected due to inefficiencies of the charge-signal collection. Furthermore, the effect on the decay energy resolution is negligible as it is determined mostly by the neutron angle resolution and the target thickness.